AGU PUBLICATIONS

Geophysical Research Letters

RESEARCH LETTER
10.1002/2014GL062359

Key Points:
- Rising frequency ramps amplify on average 1.9 times more than falling frequency ramps
- The linear growth rate as function of frequency controls initial amplification
- Higher initial growth leads to earlier onset, longer duration nonlinear growth

Supporting Information:
- Readme
- Movie S1

Correspondence to:
J. D. Li,
jdli@stanford.edu

Citation:
Li, J. D., V. Harid, M. Spasojevic, M. Gołkowski, and U. S. Inan (2015), Preferential amplification of rising versus falling frequency whistler mode signals, *Geophys. Res. Lett.*, *42*, doi:10.1002/2014GL062359.

Received 28 OCT 2014
Accepted 16 DEC 2014
Accepted article online 19 DEC 2014

Preferential amplification of rising versus falling frequency whistler mode signals

J. D. Li[1], V. Harid[1], M. Spasojevic[1], M. Gołkowski[2], and U. S. Inan[1,3]

[1]Department of Electrical Engineering, Stanford University, Stanford, California, USA, [2]Department of Electrical Engineering, University of Colorado Denver, Denver, Colorado, USA, [3]Department of Electrical Engineering, Koc University, Istanbul, Turkey

Abstract Analysis of ground-based ELF/VLF observations of injected whistler mode waves from the 1986 Siple Station experiment demonstrates the preferential magnetospheric amplification of rising over descending frequency-time ramps. From examining conjugate region receptions of ±1 kHz/s frequency-time ramps, we find that rising ramps generate an average total power 1.9 times higher than that of falling frequency ramps when both are observed during a transmission. And in 17% of receptions, only rising ramps are observed above the noise floor. Furthermore, the amplification ratio inversely correlates with the noise and total signal power. Using a narrowband Vlasov-Maxwell numerical simulation, we explore the preferential amplification due to differences in linear growth rate as a function of frequency, relative to the frequency which maximizes the linear growth rate for a given anisotropy, and in nonlinear phase trapping. These results contribute to the understanding of magnetospheric wave amplification and the preference for structured rising elements in chorus.

1. Introduction

Nonlinear cyclotron-resonant wave-particle interactions contribute to the amplification of whistler mode signals in the Earth's magnetosphere and are critical in explaining the generation of waves with narrowband frequency-time structure such as chorus, discrete emissions, and triggered emissions [*Helliwell*, 1965; *Nunn*, 1974; *Omura et al.*, 1991, 2008]. Past observational work has shown that for naturally occurring waves, a rising frequency-time structure tends to be preferentially generated and amplified in the magnetosphere. *Burtis and Helliwell* [1976] reported that 77% of chorus samples consisted of primarily rising frequency elements, and *Li et al.* [2011] showed that rising frequency chorus elements tend to have higher average amplitude (30–100 pT) than falling frequency chorus elements (<30 pT). Experiments involving the injection of waves into the magnetosphere from ground-based ELF/VLF transmitters [*Mielke and Helliwell*, 1993; *Carlson et al.*, 1985] and from modulated ionospheric heating experiments [*Gołkowski et al.*, 2008, 2010, 2011] have also noted the tendency for rising frequency ramps to be amplified to a higher degree while falling frequency ramps are weaker or absent in recordings made on the ground in the conjugate hemisphere.

From a theoretical standpoint, the trapping of electrons in the potential well of the wave is considered a necessary condition for nonlinear wave growth [*Dysthe*, 1971; *Nunn*, 1974; *Dowden et al.*, 1978; *Vomvoridis and Denavit*, 1979; *Bell and Inan*, 1981; *Omura et al.*, 1991]. The conditions for particle trapping depend in part on the frequency sweep rate of the input signal, and theoretical investigation and numerical simulation of the generation of rising and falling triggered emissions have been performed [*Omura et al.*, 2008; *Nunn and Omura*, 2012].

Wave injection experiments provide an opportunity to explore and quantify aspects of nonlinear wave-particle phenomena in a controlled manner. A major effort has recently been undertaken to restore and archive data collected in the Siple Station experiment, which operated from 1973 to 1988 [*Li et al.*, 2014]. The experiment consisted of a 500 Hz to 5 kHz transmitter located at Siple Station, Antarctica (75.93°S, 84.25°W geographic and $L = 4.2$) and, for the data used here, a receiving station in the conjugate hemisphere at Lake Mistissini, Canada (50.42°N, 73.87°W geographic). The Siple Station experiment provided a wealth of observations of nonlinear wave-particle interaction phenomena [*Helliwell*, 1979, 1988] and remains an important data source for validating theoretical and numerical models of nonlinear wave-particle interactions [*Gibby et al.*, 2008; *Hikishima and Omura*, 2012; *Nunn and Omura*, 2012]. Here

©2014. American Geophysical Union. All Rights Reserved.

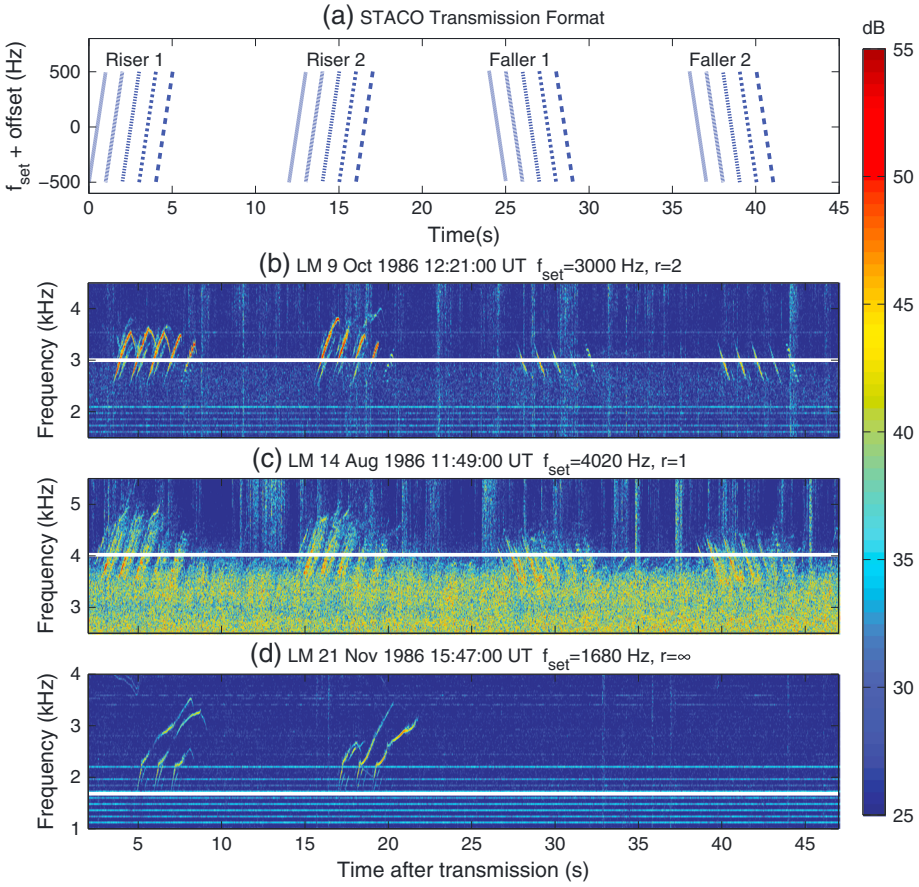

Figure 1. (a) Illustration of the STACO format transmitted by Siple and conjugate receptions with riser to faller amplification ratios of (b) $r = 2$, (c) $r = 1$, and (d) $r = \infty$.

we analyze a database of transmissions consisting of a sequence of rising and falling frequency ramps (± 1 kHz/s) and develop a metric to quantify the relative amplification of each transmission. We subsequently use a recently developed first-order, narrowband Vlasov-Maxwell solver to simulate the growth of rising and falling frequency ramps. We investigate differences in amplification by examining the differences in the linear growth rate as a function of frequency as well as the conditions for particle trapping and nonlinear growth.

2. Statistical Observations From 1986

The staircase coherence format, abbreviated STACO, transmitted by Siple Station from July to December of 1986 is illustrated in Figure 1a and is composed of two identical sets of rising, 1 kHz/s ramp elements (Riser 1 and Riser 2), followed by two identical sets of falling, −1 kHz/s ramp elements (Faller 1 and Faller 2). Each ramp set is composed of five elements that are approximations to an ideal frequency ramp using 1 ms, 10 ms, 25 ms, 50 ms, and 100 ms long tones with each ramp being 1 s in total duration. The entire transmission is centered on an operator-selected tuning frequency, f_{set}, which ranged from 1680 Hz to 4020 Hz. Data from the conjugate receiving station is available for 170 transmissions of the STACO format, and 63 receptions were detected for a 37% reception rate. Of those detected, 60 were received with sufficient signal-to-noise ratio for further analysis. The format was originally intended for studying the required time-frequency spacing to approximate a continuous frequency ramp [*Mielke and Helliwell*, 1993].

The goal of the current study is to compare the total magnetospheric amplification, which includes both the amplification of the transmission and the generation of triggered free-running emissions, resulting from the injection of rising versus falling frequency ramps. We develop a metric to calculate the total signal power generated from each set of ramp elements, and we make comparisons between rising and falling sets only within a given transmission in order to eliminate variations due to changes in background

©2014. American Geophysical Union. All Rights Reserved.

conditions. To calculate this metric, we manually identify a set of rising or falling ramps, preprocess to reduce interference from lightning-generated sferics using a sparse separation technique [*Strauss*, 2013, section 2]. Then, we apply a 75,000-point fast Fourier transform with proper scaling for the signal duration and filter the result using a 1000-point median filter to further remove impulsive noise in the frequency domain, such as power line harmonics and single-frequency fluctuations in the background noise. We integrate over a 3 kHz window centered on f_{set} and identify this number as the uncalibrated power metric for the signal using Parseval's theorem. We also apply this same methodology to a manually selected segment of data from several seconds prior to or following the ramp set to characterize the local background noise around the time of the ramp reception. This noise power is then subtracted from the signal power metric to obtain a single number for the amplification metric. The amplification ratio (r) is then the ratio of the amplification metric for different sets of ramps within a transmission, such as rising to falling or Rising 1 to Rising 2.

Figures 1b–1d show examples of receptions of the STACO format for three different amplification ratios. Figures 1b–1d are aligned in time and are shifted 3 s from Figure 1a to account for propagation delay. The first example (Figure 1b) shows a case where the rising to falling amplification ratio is about 2 and exhibits stronger amplification of the transmitted rising signals, triggered emissions (downward hooks at the top of the rising ramps), and visible multipath effects. The Siple transmissions are believed to reach the conjugate hemisphere primarily in a ducted propagation mode [*Carpenter and Sulic*, 1988], and multipath refers to the phenomenon where the transmission propagates in multiple magnetospheric ducts simultaneously. Multipath effects can be seen on the spectrograms in Figures 1b–1d as additional receptions within a 0.5 s window. In Figure 1c, the rising to falling amplification ratio is near unity, with both risers and fallers appearing similar in intensity and embedded in a band of hiss. Finally, Figure 1d is an example where the fallers are not detected (deemed $r = \infty$) while some significant portion of the risers are detected and generate rising tone-triggered emissions that extend > 1 kHz above the transmitted ramp.

The distribution of amplification ratios for all received transmissions of the STACO format is shown in Figure 2. The histogram in Figure 2a presents the amplification ratio for Riser 1 to Riser 2 sets in order to evaluate any possible difference in amplification due to temporal effects. The median value of r is 1.06 and 61% of cases have values of r between 0.75 and 1.25. The histogram in Figure 2b shows the distribution of the amplification ratio for rising to falling ramps. We note that the bin with highest occurrence ($n = 10$) is the infinite ratio bin, that is, the falling ramps are not received at all. The median value of the ratio, not including the infinite cases, is 1.93, and 12 cases (20%) have a r value less than 1, that is, fallers are amplified more than risers. Of those 12 cases, 5 cases have $r > 0.8$, 4 cases have $0.8 > r > 0.5$, and 3 cases have a $0.5 > r > 0.3$. The results from Figure 2a, that subsequent ramps have an amplification ratio near 1, suggest that the differences in the rising to falling amplification are unlikely to be due to temporal effects within a given transmission. Figure 2c shows a scatterplot of the noise power versus the rising to falling amplification ratio, where the dividing $r = 1$ line separates the two regions of differing behavior. As we have an insufficient number of cases where $r < 1$, we examine cases only where the risers are amplified more than fallers and the fallers are received (that is, $1 < r < \infty$) and find that as the noise power increases, the amplification ratio decreases. The correlation coefficient between noise power and amplification ratio in that range of r is -0.46 ($p < 0.01$). *Li et al.* [2014] reported that the primary contribution to the increase in noise power for Siple receptions is the occurrence of natural emissions such as hiss, as seen in Figure 1c, and as such, intervals of higher noise power likely indicate when the conditions for linear growth are enhanced. As applied to Figure 2c, lower noise power suggests lower linear growth rates which are then associated with higher amplification ratios. Figure 2d shows a scatterplot of the total power of the rising ramps versus the rising to falling amplification ratio with a similar trend of the rising power metric increasing as the amplification ratio decreases. We also examined the relationship between the amplification ratio and the f_{set} frequency, the *Kp* index at the time of transmission, and the local time of transmission and found no correlation.

3. Theory and Modeling

Modeling the propagation and growth of whistler mode waves interacting with energetic radiation belt electrons requires solving the Vlasov-Maxwell system of equations. The evolution of the electron distribution function is governed by the Vlasov equation while the wave fields are generated according to Maxwell's equations. Under the assumption of parallel propagating signals, which ducted Siple signals are considered to be, the interaction between waves and particles is dominated by cyclotron resonance. For small amplitude injected waves, the solution to the Vlasov-Maxwell system according to linear theory

©2014. American Geophysical Union. All Rights Reserved.

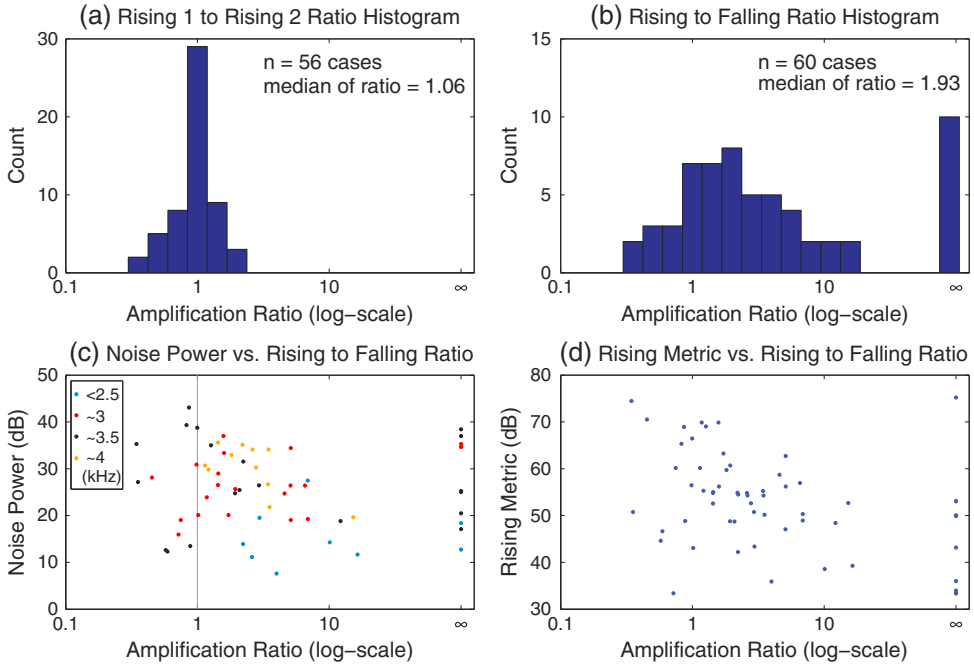

Figure 2. Results from the statistical analysis of the STACO format. The histograms show (a) the amplification ratio between the sequential rising sets, Riser 1 and Riser 2, and (b) the amplification ratio between rising and falling sets with the amplification ratios on a log scale. The scatterplots show the log-scale riser to faller amplification ratio as functions of (c) the noise power metric (color coded by the value of f_{set}) and (d) the riser amplification metric.

predicts exponential wave growth if the electron distribution is sufficiently anisotropic [*Kennel and Petschek*, 1966]. Although the linear growth rate is a function of frequency, linear growth of rising and falling frequency ramps sweeping over the same frequency range will result in the same net integrated amplification, and thus, variations in the linear growth rate with frequency cannot explain the preferential amplification of rising ramps observed in the data. However, after undergoing linear growth, the wave amplitudes can become large enough to trap resonant electrons in the wave potential well, and the formation of this trap is believed to play a crucial role in nonlinear wave growth [*Nunn*, 1974; *Dowden et al.*, b1978; *Vomvoridis and Denavit*, 1979; *Bell and Inan*, 1981; *Omura et al.*, 1991]. The conditions for particle trapping can be summarized by a single collective inhomogeneity parameter, *S*, [*Omura et al.*, 1991] defined as follows:

$$S = \frac{1}{2\omega_t^2}\left[\left(3V_R - \frac{kv_\perp^2}{\omega_c}\right)\frac{\partial\omega_c}{\partial z} - \frac{2\omega + \omega_c}{\omega}\frac{\mathrm{d}\omega}{\mathrm{d}t}\right] \tag{1}$$

with the quantities ω_c, ω, and k representing the electron gyrofrequency, wave frequency, and wave number, respectively. V_R is the resonance velocity, and $v_\perp$ is the component of the particle velocity perpendicular to the geomagnetic field, which is oriented in the z direction. The quantity ω_t is the trapping frequency defined as follows:

$$\omega_t = \left(\frac{qv_\perp kB_w}{m_e}\right)^{\frac{1}{2}} \tag{2}$$

where B_w is the wave magnetic field, q is the magnitude of the electron charge, and m_e is the electron mass.

When S has a magnitude less than 1, particle trapping and consequently nonlinear wave growth can occur. As shown in equation (1), S depends on the inhomogeneity of the geomagnetic field $\left(\frac{\partial\omega_c}{\partial z}\right)$ as well as on the frequency sweep rate of the wave $(\frac{\mathrm{d}\omega}{\mathrm{d}t})$. For simplicity, we first consider the hypothetical case of a constant amplitude wave. The center of the interaction region is defined at $S = 0$, and the extent of the interaction region is defined where $|S| < 1$. For a monochromatic wave, $\|S(z)\|$ is symmetric around the equator, and thus, the nonlinear interaction region is also symmetric around the equator. For a rising frequency ramp,

©2014. American Geophysical Union. All Rights Reserved.

$\frac{\partial w}{\partial t}$ is a positive constant, and $S(z)$ thus resembles the monochromatic profile except that it is shifted upstream to latitudes toward the transmitter. Likewise, the reverse scenario holds true for a falling frequency ramp, and the nonlinear interaction region shifts downstream toward the receiver. For the case of a constant amplitude wave, the spatial shift in the interaction region is approximately symmetric around the equator for rising and falling tones. The inclusion of wave amplification adds to the complexity as ω_t depends on the wave amplitude, and the wave amplitude will be growing as a function of position along the magnetic field line, which then changes the value of S; this is an important aspect that contributes to the difference in amplification of rising compared to falling ramps.

3.1. Numerical Model

Modeling nonlinear amplification of coherent waves is analytically intractable and must be approached using numerical techniques. The Vlasov equation in canonical coordinates is shown in equation (3), where the terms $\frac{dx_i}{dt}$ are governed by the single-particle equations of motion, the Lorentz force.

$$\frac{\partial f}{\partial t} + \sum_{i=1}^{n} \frac{dx_i}{dt} \frac{\partial f}{\partial x_i} = 0 \tag{3}$$

In this study, we simulate the amplification of rising and falling frequency ramps using a recently developed narrowband Vlasov solver [*Harid et al.*, 2014]. The solver discretizes the Vlasov equation on a uniform phase-space grid and then integrates in time using a first-order finite difference linear upwind scheme. The model is well suited for simulating the growth of coherent waves in the large amplitude regime where particle phase-trapping dominates.

Since the waves in this simulation are coherent, the Vlasov equation can be coupled to the narrowband wave equations shown in equations (4) and (5), which also account for the background cold plasma [*Nunn*, 1974].

$$\frac{\partial B_w}{\partial t} - v_g \frac{\partial B_w}{\partial z} = -\frac{\mu_0 v_g}{2} J_E \tag{4}$$

$$\frac{\partial \phi_w}{\partial t} - v_g \frac{\partial \phi_w}{\partial z} = -\frac{\mu_0 v_g}{2} \frac{J_B}{B_w} \tag{5}$$

The quantities B_w and ϕ_w are the wave amplitude and phase of the modulating wave packet propagating in the $-z$ direction at the group velocity, v_g. J_E and J_B are components of the resonant current in the direction of the wave electric and magnetic fields, respectively. The narrowband wave equations are integrated in time with the same finite difference scheme used for the Vlasov equation.

To simulate the Siple transmissions, we use a centered dipole geomagnetic field model at $L = 4$ and a cold plasma density of 250 cm^{-3}. The hot plasma distribution function is a bi-Maxwellian with a temperature anisotropy $\left(A = \left(\frac{T_\perp}{T_\parallel}\right) - 1\right)$ of 1.16 and a hot electron density (n_h) of 0.25 cm^{-3}. The simulation domain extends out ±5000 km around the equator, chosen based on the minimum trapping amplitude threshold parameterized by S and for consistency with past work [*Nunn*, 1974; *Gibby et al.*, 2008]. Pulses that rise or fall in frequency are injected into the simulation space by enforcing a chirped phase at the input with an initial amplitude of 0.1 pT. The input pulses are 0.5 s in duration, and the rising and falling ramps have equal though opposite sweep rates, cover the same 500 Hz range of frequencies, and have the same center frequency. The instantaneous frequency profile for the rising ramps is given by $f_{\text{rise}}(t) = (f_{\text{set}} - 250) + 1000t$ and for the falling ramps by $f_{\text{fall}}(t) = (f_{\text{set}} + 250) - 1000t$, where f_{set} is the center frequency of the ramp. The linear growth spectrum for the simulation parameters is shown in Figure 3a, and a family of linear growth rate curves for varying anisotropies is shown in Figure 3b. In Figure 3a, the frequency at which the linear growth rate is maximized (f_m) is 2450 Hz, and the center frequencies for the simulation are chosen such that two frequencies are below f_m (1000 Hz and 1500 Hz), and the other two are above f_m (3480 Hz and 4500 Hz). Linear growth alone cannot explain the difference between rising and falling ramps; however, all signals first undergo linear growth before crossing the nonlinear threshold. Therefore, rising ramps with a center frequency above the maximum linear growth rate frequency will at first grow faster than falling ramps as the starting frequency is closer to f_m and subsequently reach the nonlinear threshold sooner. We thus expect

©2014. American Geophysical Union. All Rights Reserved.

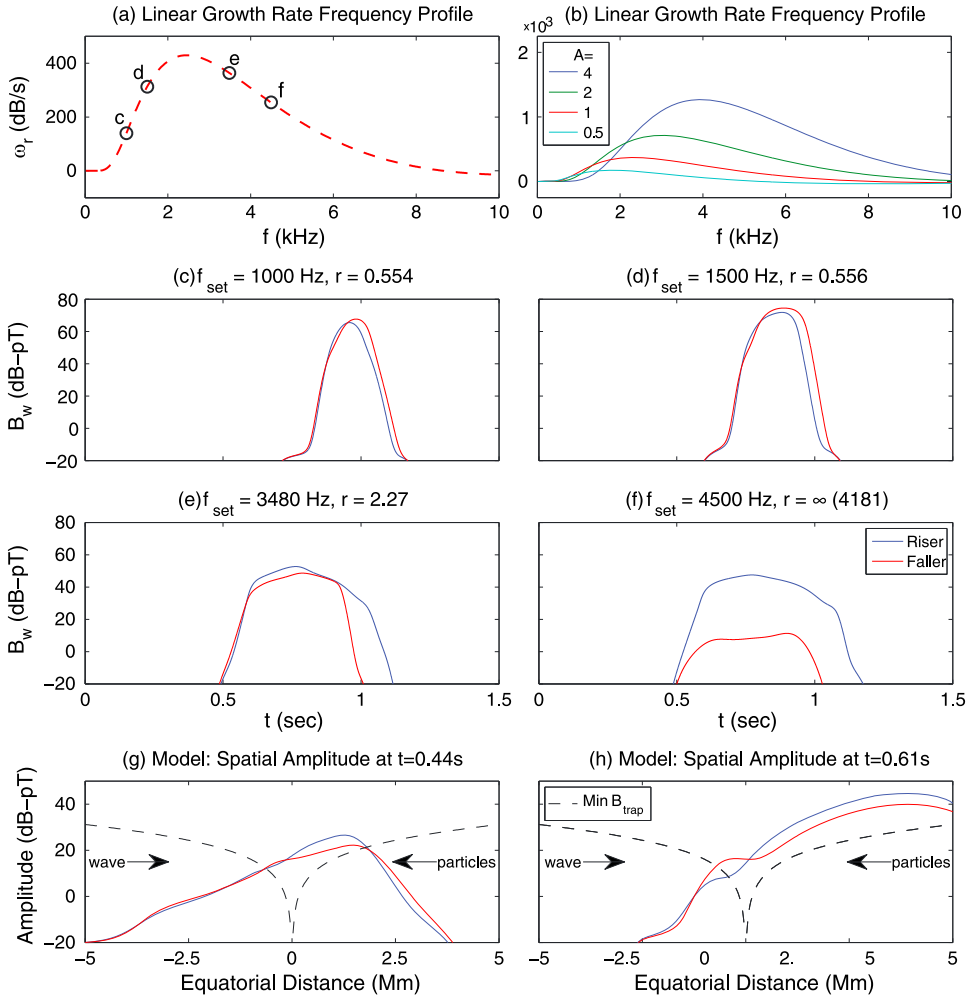

Figure 3. (a) The linear growth rate curve as a function of wave frequency for $A = 1.16$ and $n_h = 0.25$ cm^{-3} with four points indicating the center frequency for the simulation in the corresponding panel and (b) as a family of such curves for a range of anisotropies. The time series plots show the simulated amplitude at the end of the interaction region ($z = 5000$ km) for (c) $f_{set} = 1000$ Hz, (d) $f_{set} = 1500$ Hz, (e) $f_{set} = 3480$ Hz, and (f) $f_{set} = 4500$ Hz for risers (blue) and fallers (red). Additionally, the spatial amplitude profile over the interaction region is shown at (g) $t = 0.44s$ and at (h) $t = 0.61$ s for risers (blue) and fallers (red), with the minimum trapping amplitude for a monochromatic wave with 70° pitch angle (black).

rising ramps to amplify more in these cases and falling ramps to amplify more in the cases where the center frequency is below the maximum linear growth rate frequency.

The received wave amplitudes for the fully nonlinear simulations are shown in Figures 3c–3f, plotted as a function of time at the output of the simulation space ($z = 5000$ km). For the two cases where the center frequency is below f_m, Figures 3c and 3d, the falling ramps grow more than the rising ramps. The corresponding amplification ratios (riser to faller) are 0.554 and 0.556 for the 1000 Hz and 1500 Hz cases, respectively. Figures 3e and 3f, with center frequencies of 3480 Hz and 4500 Hz, correspond to the cases where the rising ramp grows faster at first due to the higher initial linear growth rate and thus reaches the trapping threshold sooner. The corresponding amplification ratios are 2.27 for $f_{set} = 3480$ Hz and 4181 for $f_{set} = 4500$ Hz. In fact, for the 4500 Hz case (Figure 3f), the falling ramp does not reach the trapping threshold and does not undergo any nonlinear growth and subsequently gives a far lower output amplitude than the rising ramp and thus a very large amplification ratio, matching well with the infinity ratio cases.

The fact that Siple observations generally show a higher degree of growth for rising ramps suggests that the transmitted signals are more likely to be above f_m. Further, as seen in Figure 3b, when the electron temperature anisotropy decreases, the value of f_m decreases. Thus, lower anisotropies will favor the growth

©2014. American Geophysical Union. All Rights Reserved.

of risers, as more of the spectrum is above f_m. This is consistent with the observational finding in Figure 2c showing that lower noise power (which is associated with less natural emissions and presumably a lower linear growth rate) favors higher amplification ratios (better amplification of risers). As A decreases, risers are favored, but the total growth of signals is expected to be lower, and this trend is seen in Figure 2d where higher amplification of risers over fallers is associated with lower total power in the risers.

Spatial amplitude profiles from the simulation shown in Figure 3e with f_{set} = 3480 Hz are shown at two different time steps in the simulation in Figures 3g and 3h, with an animation of all of the full simulations in the supplementary materials. The dashed curve represents the minimum amplitude for particle trapping for a monochromatic tone at f_{set}. At $t = 0.44$ s in Figure 3g, in the region upstream of the equator ($z < 0$), the waves are below the minimum trapping amplitude and grow according to linear theory. The linear growth rate, which is a function of the wave frequency, is initially higher for the rising tone as it starts at a lower frequency. This difference in initial linear growth rates ensures that the rising tone crosses the minimum trapping amplitude sooner than the falling tone and consequently undergoes nonlinear growth sooner as well.

At a later time ($t = 0.61$ s), shown in Figure 3h, the waves have propagated further through the simulation space. The wave amplitude of the falling ramp is still lower than the rising ramp; however, the falling ramp has grown in time such that the wave crosses the minimum trapping amplitude. This occurs due to the increase in linear growth rate resulting from the decrease in the falling ramp frequency and partially from the accompanying shift of the nonlinear interaction region downstream. Conversely, the rising ramp begins to damp slightly near ($z = 0$) because the linear growth rate has decreased due to the increased frequency; however, since the riser crossed the trapping threshold earlier in time, the change in the linear growth rate does not play as much of a role. The net effect is that the rising ramp undergoes more amplification than the falling frequency ramp.

4. Conclusions

Historical observations of Siple Station transmissions [*Mielke and Helliwell*, 1993; *Carlson et al.*, 1985], along with more recent cases from HAARP wave injection experiments [*Gołkowski et al.*, 2008, 2011] and satellite recordings of discrete chorus elements [*Burtis and Helliwell*, 1976; *Li et al.*, 2011], indicate a natural preference for the amplification of rising frequency signals over falling frequency signals. Furthermore, the importance of the time and location of the transition from linear to nonlinear growth was postulated from wave injection observations made by *Gołkowski et al.* [2010].

Here, for the first time, we quantify the amplification of rising and falling frequency ramps injected into the magnetosphere from Siple Station and use a narrowband Vlasov-Maxwell simulation to interpret the results. Simulations show that the net amplification of frequency ramps depends on both the linear growth rate and the duration of nonlinear growth. When the center frequency of the ramp is above f_m, the frequency at which the linear growth rate is maximized, rising frequency ramps will undergo more initial linear growth. Conversely, falling frequency ramps will undergo more initial growth when the center frequency is below f_m. Further, for rising frequency ramps the nonlinear interaction region is shifted upstream (to latitudes below the equator for a Southern Hemisphere transmitter), and thus, rising ramps can undergo nonlinear growth earlier and for a longer duration owing to the feedback effect of wave amplitude on the conditions for nonlinear growth (such as expressed in the S parameter). These effects combine to result in a net preferential amplification of rising frequency ramps. In the Siple receptions, we find that rising frequency ramps generate a total power that is on average 1.9 times higher than that of falling frequency ramps when both are received within a given transmission. Also, in 17% of receptions, only the rising frequency ramps are observed, and the falling ramps are below the detectable signal level. This may occur when the falling ramps do not reach the threshold for nonlinear growth such as when the ramp center frequency is well above f_m as in Figure 3f. A lower value of hot electron temperature anisotropy will move f_m to lower frequency, further favoring the growth of rising ramps. This is supported observationally by the inverse correlation between the amplification ratio and both the observed noise power and the total signal power metric. Finally, in 20% of the receptions, falling ramps are amplified more than rising ramps, and simulations show that this may occur when the ramp center frequency is below f_m. Our results contribute to the understanding of magnetospheric wave amplification, and the described mechanism likely also plays a role in chorus emissions, which likewise exhibit a preference for structured rising as opposed to falling emissions.

©2014. American Geophysical Union. All Rights Reserved.

Acknowledgments
This work is supported by AFRL award FA9453-11-C-0011 to Stanford University and subcontract 27239350-50917-B to CU Denver. Mark Gołkowski acknowledges additional support from NSF CAREER award 1254365. We are grateful to Yoshiharu Omura, Timothy Bell, and Donald Carpenter for helpful discussions. We thank Dominic Delgado for his help in preprocessing portions of the data set. Requests for the data used for analysis and for the simulation code and results can be directed to the corresponding author.

The Editor thanks David Nunn and an anonymous reviewer for their assistance in evaluating this paper.

References

Bell, T. F., and U. S. Inan (1981), Transient nonlinear pitch angle scattering of energetic electrons by coherent VLF wave packets in the magnetosphere, *J. Geophys. Res.*, *86*, 9047–9063, doi:10.1029/JA086iA11p09047.

Burtis, W. J., and R. A. Helliwell (1976), Magnetospheric chorus—Occurrence patterns and normalized frequency, *Planet. Space Sci.*, *24*, 1007–1024, doi:10.1016/0032-0633(76)90119-7.

Carlson, C. R., R. A. Helliwell, and D. L. Carpenter (1985), Variable frequency VLF signals in the magnetosphere Associated phenomena and plasma diagnostics, *J. Geophys. Res.*, *90*, 1507–1521, doi:10.1029/JA090iA02p01507.

Carpenter, D. L., and D. M. Sulic (1988), Ducted whistler propagation outside the plasmapause, *J. Geophys. Res.*, *93*, 9731–9742, doi:10.1029/JA093iA09p09731.

Dowden, R. L., A. D. McKay, L. E. S. Amon, H. C. Koons, and M. H. Dazey (1978), Linear and nonlinear amplification in the magnetosphere during a 6.6-kHz transmission, *J. Geophys. Res.*, *83*(A1), 169–181, doi:10.1029/JA083iA01p00169.

Dysthe, K. B. (1971), Some studies of triggered whistler emissions, *J. Geophys. Res.*, *76*(28), 6915–6931, doi:10.1029/JA076i028p06915.

Gibby, A. R., U. S. Inan, and T. F. Bell (2008), Saturation effects in the VLF-triggered emission process, *J. Geophys. Res.*, *113*, A11215, doi:10.1029/2008JA013233.

Gołkowski, M., U. S. Inan, A. R. Gibby, and M. B. Cohen (2008), Magnetospheric amplification and emission triggering by ELF/VLF waves injected by the 3.6 MW HAARP ionospheric heater, *J. Geophys. Res.*, *113*, A10201, doi:10.1029/2008JA013157.

Gołkowski, M., U. S. Inan, M. B. Cohen, and A. R. Gibby (2010), Amplitude and phase of nonlinear magnetospheric wave growth excited by the HAARP HF heater, *J. Geophys. Res.*, *115*, A00F04, doi:10.1029/2009JA014610.

Gołkowski, M., M. B. Cohen, D. L. Carpenter, and U. S. Inan (2011), On the occurrence of ground observations of ELF/VLF magnetospheric amplification induced by the HAARP facility, *J. Geophys. Res.*, *116*, A04208, doi:10.1029/2010JA016261.

Harid, V., M. Gołkowski, T. Bell, J. D. Li, and U. S. Inan (2014), Finite difference modeling of coherent wave amplification in the Earth's radiation belts, *Geophys. Res. Lett.*, *41*, doi:10.1002/2014GL061787.

Helliwell, R. A. (1965), *Whistlers and Related Ionospheric Phenomena*, Stanford Univ. Press, Stanford, Calif.

Helliwell, R. A. (1979), Siple station experiments on wave-particle interactions in the magnetosphere, in *Wave Instabilities in Space Plasmas*, edited by P. J. Palmadesso and K. Papadopoulos, pp. 191–203, D Reidel, Dordrecht, Netherlands.

Helliwell, R. A. (1988), VLF wave-injection experiments from Siple Station, Antarctica, *Adv. Space Res.*, *8*, 279–289, doi:10.1016/0273-1177(88)90373-0.

Hikishima, M., and Y. Omura (2012), Particle simulations of whistler-mode rising-tone emissions triggered by waves with different amplitudes, *J. Geophys. Res.*, *117*, A04226, doi:10.1029/2011JA017428.

Kennel, C. F., and H. E. Petschek (1966), Limit on stably trapped particle fluxes, *J. Geophys. Res.*, *71*(1), 1–28, doi:10.1029/JZ071i001p00001.

Li, J. D., M. Spasojevic, V. Harid, M. B. Cohen, M. Gołkowski, and U. Inan (2014), Analysis of magnetospheric ELF/VLF wave amplification from the Siple Transmitter experiment, *J. Geophys. Res. Space Physics*, *119*, 1837–1850, doi:10.1002/2013JA019513.

Li, W., R. M. Thorne, J. Bortnik, Y. Y. Shprits, Y. Nishimura, V. Angelopoulos, C. Chaston, O. Le Contel, and J. W. Bonnell (2011), Typical properties of rising and falling tone chorus waves, *Geophys. Res. Lett.*, *38*, L14103, doi:10.1029/2011GL047925.

Mielke, T. A., and R. A. Helliwell (1993), Siple Station, Antarctica, experiments on staircase frequency ramps as approximations to continuous ramps, *J. Geophys. Res.*, *98*, 4053–4061, doi:10.1029/92JA02562.

Nunn, D. (1974), A self-consistent theory of triggered VLF emissions, *Planet. Space Sci.*, *22*(3), 349–378, doi:10.1016/0032-0633(74)90070-1.

Nunn, D., and Y. Omura (2012), A computational and theoretical analysis of falling frequency VLF emissions, *J. Geophys. Res.*, *117*, A08228, doi:10.1029/2012JA017557.

Omura, Y., D. Nunn, H. Matsumoto, and M. J. Rycroft (1991), A review of observational, theoretical and numerical studies of VLF triggered emissions, *J. Atmos. Terr. Phys.*, *53*(5), 351–368, doi:10.1016/0021-9169(91)90031-2.

Omura, Y., Y. Katoh, and D. Summers (2008), Theory and simulation of the generation of whistler-mode chorus, *J. Geophys. Res.*, *113*, A04223, doi:10.1029/2007JA012622.

Strauss, D. (2013), Electromagnetic subsurface imaging at VLF with distributed optimization, PhD dissertation, Stanford Univ., Stanford, Calif.

Vomvoridis, J. L., and J. Denavit (1979), Test particle correlation by a whistler wave in a nonuniform magnetic field, *Phys. Fluids*, *22*(2), 367–377, doi:10.1063/1.862589.

©2014. American Geophysical Union. All Rights Reserved.